A novel accurate representation of a double-valued potential energy surface by the DMBE method. Application to triplet H3+(a3E′)

3 AUTHORS, INCLUDING:

Antonio J. C. Varandas
University of Coimbra
382 PUBLICATIONS   **6,733** CITATIONS

SEE PROFILE

Alexander Alijah
Université de Reims Champagne-Ardenne
79 PUBLICATIONS   **1,080** CITATIONS

SEE PROFILE

A novel accurate representation of a double-valued potential energy surface by the DMBE method. Application to triplet $H_3^+(a^3E')$

António J.C. Varandas [*], Alexander Alijah, Mihail Cernei

Departamento de Química, Universidade de Coimbra, 3004-535 Coimbra, Portugal

Dedicated to the memory of G.D. Billing

Abstract

Standard single-valued double many-body expansion (DMBE) theory has been extended to allow an accurate representation of a double-valued potential energy surface. With this new theory, the degeneracy of the two sheets along the conical intersection line can be guaranteed by construction. The method has been applied to the lowest triplet state of $H_3^+(a^3E')$ for which the lowest vibrational levels have also been calculated.
© 2004 Elsevier B.V. All rights reserved.

1. Introduction

In two recent publications [1,2] we have studied the potential energy surfaces of the two lowest triplet states of H_3^+. These two states become degenerate at equilateral triangular configurations and are thus connected by a conical intersection. Nearly independent analytical representations of the two sheets were obtained in the above-mentioned publications, the only restriction being that the linear energy splitting between the two surfaces in the vicinity of the intersection line be described correctly. No attempt was made to guarantee the degeneracy of the two states along the intersection line. While in principle this degeneracy should be an automatic outcome of the individual fits, in practice we have to live with a certain untidiness. That is, very small and harmless inaccuracies may have to be allowed, as it has indeed been observed. We have now devised a theoretical method for the representation of a double-valued potential energy surface that ensures the degeneracy at the intersection line to any degree of accuracy that may be required by using a single-valued like formalism. In

the present paper, we have applied this new theory, which is based on the double many-body expansion (DMBE) method, to the two sheets of triplet $H_3^+(a^3E')$.

2. Single-valued like DMBE representation of a double-valued surface

In the following, the basic formalism of single-valued DMBE theory [3] and the necessary modifications to obtain an accurate representation of a double-valued potential energy surface will be discussed. For a general multivalued DMBE approach, see [4,5].

For a triatomic molecule, the potential energy surface can be expanded as a sum of one-body, two-body and three-body terms

$$V(\mathbf{R}) = \sum_{i=1}^{3} V_i^{(1)} + \sum_{i=1}^{3} V^{(2)}(R_i) + V^{(3)}(\mathbf{R}), \qquad (1)$$

where $\mathbf{R} = \{R_1, R_2, R_3\}$ denotes the full set of interparticle distances. The sum of the three one-body terms corresponds to the energy of the three separated particles and thus provides a constant energy shift. Each of the many-body terms is then further split into two parts, which describe the extended Hartree–Fock and dynamical correlation energies, as

[*] Corresponding author. Tel./fax: +351239835867.
  E-mail addresses: varandas@qtvs1.qui.uc.pt (A.J.C. Varandas), alijah@ci.uc.pt (A. Alijah).

$$V^{(2)}(R_i) = V_{\text{EHF}}^{(2)}(R_i) + V_{\text{dc}}^{(2)}(R_i) \qquad (2)$$

and

$$V^{(3)}(\mathbf{R}) = V_{\text{EHF}}^{(3)}(\mathbf{R}) + V_{\text{dc}}^{(3)}(\mathbf{R}). \qquad (3)$$

The dynamical correlation terms are represented analytically [6] as

$$V_{\text{dc}}^{(2)}(R) = \sum_n \chi_n(R) C_n R^{-n} \qquad (4)$$

and

$$V_{\text{dc}}^{(3)}(\mathbf{R}) = \sum_{i=1}^{3} f_i(\mathbf{R}) \sum_n \chi_n(r_i) C_n r_i^{-n}. \qquad (5)$$

In the latter equation, r_i denotes the distance between the third particle and the centre of mass of particles one and two, as defined in the Jacobi coordinate system with index i. In turn,

$$f_i(\mathbf{R}) = \frac{1}{2}\{1 - \tanh[\xi(\eta s_i - s_j - s_k)]\} \qquad (6)$$

is the corresponding switching function, with (i, j, k) cyclic permutations of $(1, 2, 3)$ and the $s_i = R_i - R_{\text{ref}}$. This switching function ensures proper weighting of the three contributions $i = 1, 2, 3$ in Eq. (5) when a particular atom-diatom dissociation channel is reached. In the expressions for the dynamical correlation energies, Eqs. (4) and (5), damping functions χ_n are needed to make those terms behave at short range. These damping functions are expressed analytically as [7]

$$\chi_n(R) = \left[1 - \exp\left(-A_n \frac{R}{\rho} - B_n \frac{R^2}{\rho^2}\right)\right]^n, \qquad (7)$$

where A_n and B_n are the auxiliary functions

$$A_n = \alpha_0 n^{-\alpha_1} \quad B_n = \beta_0 e^{-\beta_1 n} \qquad (8)$$

with parameters $\alpha_0 = 16.36606$, $\alpha_1 = 0.70172$, $\beta_0 = 17.19338$ and $\beta_1 = 0.09574$. The variable ρ in Eq. (7) is defined as

$$\rho = 5.5 + \lambda R_0, \qquad (9)$$

where $R_0 = 2\sqrt{3}$ is Le Roy's [8] parameter and λ is a variational parameter.

In two previous papers [1,2], we have applied DMBE theory to model separately the lower and upper sheets of the triplet H_3^+ Jahn–Teller system. The EHF three-body term was split into two parts [9],

$$V_{\text{EHF},u/l}^{(3)}(\mathbf{R}) = \left[P_{1,u/l}^{N}(\Gamma_1, \Gamma_2, \Gamma_3) \pm \Gamma_2 P_{2,u/l}^{M}(\Gamma_1, \Gamma_2, \Gamma_3)\right] \\ \times T(\Gamma_1) \qquad (10)$$

the second of which is proportional to the Jahn–Teller type coordinate [10] Γ_2. In the above equation, the $P_{1,2}^{I}$ are polynomials of order I,

$$P_n^{I}(\Gamma_1, \Gamma_2, \Gamma_3) = \sum_{i+2j+3k \leqslant I} c_{ijk}^n \Gamma_1^i \Gamma_2^j \Gamma_3^k \qquad (11)$$

and $T(\Gamma_1)$ is a range determining factor, chosen as $T(\Gamma_1) = T_2(\Gamma_1)$ (see [1]), where

$$T_2(x) = \left[1 + e^{\gamma(x-x_0)}\right]^{-1}. \qquad (12)$$

The Γ_i are the coordinates of the integrity basis [11] and are defined as [1]

$$\Gamma_1 = Q_1, \quad \Gamma_2^2 = Q_2^2 + Q_3^2, \quad \Gamma_3^3 = Q_3(Q_3^2 - 3Q_2^2), \qquad (13)$$

where the Q_i are the usual symmetry coordinates [1,12,13], i.e. symmetry adapted linear combinations of the expansion coordinates $\tilde{R}_i$, for which in turn we use the Morse displacement coordinates [14]

$$\tilde{R}_i = \{1 - \exp[-\beta(R_i/R_0 - 1)]\}/\beta. \qquad (14)$$

Looking at the analytical form of the three-body EHF term, Eq. (10), one might think that the degeneracy of the two sheets of the potential energy surface at the intersection line can be enforced by a consistent choice of coefficients of the first polynomials, $P_{1,u/l}^{N}$. Such a procedure would work if the one-body and two-body contributions to the two sheets were identical at the intersection line, which in general is not the case. In the present system, for example, the two-body potentials of the lower sheet belong to the electronic ground state of H_2^+, $X^2\Sigma_g^+$, while those of the upper sheet belong to the repulsive $b^3\Sigma_u^+$ state of H_2. Fortunately, there is a remedy: we need to invalidate the two-body contributions at the intersection line and to fold them into the three-body EHF term. To this end the three-body EHF terms of the upper and lower surfaces are expressed as

$$V_{\text{EHF},u/l}^{(3)}(\mathbf{R}) = \bar{V}_{\text{EHF},u/l}^{(3)}(\mathbf{R}) \\ - \sum_{i=1}^{3} V_{u/l}^{(2)}(R_i)\, e^{-f(\Gamma_1, \Gamma_2, \Gamma_3)} T(\Gamma_1), \qquad (15)$$

where the three diatomic potentials are to be multiplied with some function that takes the numerical value of one at the intersection, to counteract the two-body term in the expansion Eq. (1), but that otherwise tends to zero smoothly and rapidly. Such a function may be written as $e^{-f(\Gamma_1, \Gamma_2, \Gamma_3)}$, where $f(\Gamma_1, \Gamma_2, \Gamma_3)$ is a polynomial in which the coefficients that depend only on the symmetric stretch coordinate Γ_1 and the coefficient of the constant term are zero. In its simplest form this polynomial might be

$$f(\Gamma_1, \Gamma_2, \Gamma_3) = c\Gamma_2 \qquad (16)$$

a form which we have used in the present work. Note that the two-body functions in Eq. (15) could be either the complete functions of Eq. (2), which include the EHF and the dynamical correlation terms, or just the

---

[1] Note that in previous papers [1,2] the definition of Γ_2 and Γ_3 is incorrect and that, in Eq. (17) of [1] and Eq. (11) of [2], the $\sqrt{\Gamma_2}$ should be replaced by Γ_2. Such changes have no implications on results reported there that were calculated using the correct expressions.

EHF terms, since the dynamical correlation contributions are identical for the two sheets. Due to the non-polynomial character of these dynamical correlation terms, the latter option is to be preferred. The EHF three-body functions $\bar{V}_{\text{EHF},u/l}^{(3)}$, that have been defined through Eq. (15), can now be written in the desired form, which is

$$\bar{V}_{\text{EHF},u/l}^{(3)}(\mathbf{R}) = \left[\bar{P}_{1,u/l}^{N}(\Gamma_1, \Gamma_2, \Gamma_3) \right.$$
$$\left. \pm \Gamma_2 \bar{P}_{2,u/l}^{M}(\Gamma_1, \Gamma_2, \Gamma_3) \right] T(\Gamma_1) \qquad (17)$$

with the positive sign referring to the upper sheet and the negative to the lower, respectively. The contribution of the two-body functions at the intersection line, which has been subtracted in Eq. (15), is included in the definition of the polynomials $\bar{P}_{1,u/l}^{N}(\Gamma_1, \Gamma_2, \Gamma_3)$, so that the two expressions for the three-body EHF terms, the conventional one, Eq. (10), and the new one, Eq. (15), are equivalent.

After these modifications, the two sheets of the potential energy surface can be joined exactly. This is subject to the following two conditions: The first is that the two sheets become degenerate along the intersection line, which requires that those coefficients in the first polynomials of Eq. (17) depending only on the symmetric stretch coordinate Γ_1 be identical for the two sheets, i.e.,

$$c_{i00,u}^{1} = c_{i00,l}^{1} \quad \forall i. \qquad (18)$$

The second matching condition concerns the slope along the Jahn–Teller type coordinate, since in the vicinity of the intersection the splitting between the two sheets must be a linear function of this coordinate [10]. This second condition leads to the obvious constraint

$$c_{000,u}^{2} = c_{000,l}^{2} \qquad (19)$$

for the coefficients of the constant terms in the second polynomials of Eq. (17).

Outside the region in which the three-body EHF term is active, the degeneracy of the two surfaces along the intersection line is no longer guaranteed by the analytical form of the expansion of the surfaces. However, in this region the diatomic potential curves are expected to be close to their asymptotic limits, so that the energy difference between them, which spoils the degeneracy, is very small. The active region of the three-body EHF term is controlled by the range determining factor $T(\Gamma_1)$.

3. Ab initio calculations and fitting procedure

The electronic ab initio data points for the two sheets were calculated in C_s symmetry with the MOLPRO package [15]. A full CI was performed in the large basis of 165 functions generated from Dunning's cc-pV5Z basis set [16]. The potential energy surfaces of H_3^+ have a threefold symmetry due to the three equivalent nuclei.

Each of the three sectors contains two equivalent parts which are related by reflection through a plane of symmetry. It is thus sufficient to calculate the data points in just one sixth of the configuration space. A convenient grid can be defined in the hyperspherical coordinates [17,18] ρ, θ and ϕ, from which the interparticle distances are then obtained as

$$R_1^2 = \frac{\rho^2}{\sqrt{3}}[1 + \sin\theta \sin(\phi + 4\pi/3)],$$

$$R_2^2 = \frac{\rho^2}{\sqrt{3}}[1 + \sin\theta \sin(\phi - 4\pi/3)], \qquad (20)$$

$$R_3^2 = \frac{\rho^2}{\sqrt{3}}[1 + \sin\theta \sin\phi].$$

For fixed values of the hyperradius ρ, the hyperangles θ and ϕ were varied within $0° \leqslant \theta \leqslant 90°$ and $30° \leqslant \phi \leqslant 90°$, with increments of $\Delta\theta = 5°$ and $\Delta\phi = 5°$. In our previous work [1,2] we mainly used the data points from [19], which are for $\rho = 3.0, 3.5, 4.0, 4.5, 5.0, 5.5, 6.0, 7.0, 8.0, 9.0$ and 10.0. In the course of this work it was found necessary to extend the range of the three-body term and thus to augment the base of data points used previously. Further ab initio points were calculated for values of the hyperradius $\rho = 11.0, 12.0, 14.0, 16.0, 18.0$ and 20.0 and along the intersection line. The total number of data points was 3621 for each sheet of the surface. These points cover one-sixth of the configuration space which, due to the high symmetry of the potential as explained above, is representative for the complete configuration space.

With the extended data base we have obtained new fits for the two sheets of the a^3E' surface, employing the novel functional forms suggested in this work. The parameters to be determined in a least squares procedure are those of the three-body term including the correction function with which the two-body terms are multiplied. As described before [1], we define a function $\epsilon_{u/l}(\mathbf{R}_n)$ as

$$\epsilon_{u/l}(\mathbf{R}_n) = E_{u/l}(\mathbf{R}_n) - \sum_{i=1}^{3} V_i^{(1)} - \sum_{i=1}^{3} V^{(2)}(R_{i,n})$$
$$- V_{\text{dc}}^{(3)}(\mathbf{R}_n). \qquad (21)$$

In the above equation, we denoted by $\mathbf{R}_n$, $n = 1, \ldots, N$ the ab initio data points, each of which being defined by the three interparticle distances $R_{i,n}$, $i = 1, 2, 3$, and by $E_{u/l}(\mathbf{R}_n)$ the corresponding ab initio data of the electronic energy of the upper and lower state, respectively. Minimisation of the functions

$$\chi_{u/l}^2 = \sum_{n=1}^{N} \left[\epsilon_{u/l}(\mathbf{R}_n) - V_{\text{EHF},u/l}^{(3)}(\mathbf{R}_n) \right]^2 \qquad (22)$$

$$= \sum_{n=1}^{N} \left[\epsilon_{u/l}(\mathbf{R}_n) - \left(\bar{V}_{\text{EHF},u/l}^{(3)}(\mathbf{R}_n) \right. \right.$$
$$\left. \left. - \sum_{i=1}^{3} V_{u/l}^{(2)}(R_{i,n}) e^{-f(\Gamma_1, \Gamma_2, \Gamma_3)} T(\Gamma_1) \right) \right]^2 \qquad (23)$$

with respect to the parameters of the functions $f(\Gamma_1, \Gamma_2, \Gamma_3)$ and $\bar{V}^{(3)}_{\text{EHF},u/l}(\mathbf{R}_n)$ of the three-body EHF term yields their numerical values.

To obtain consistent representations of the two sheets, the corresponding least squares fits were performed simultaneously. For the fit of the lower sheet all 3621 data points were used, while for that of the upper sheet the points with extremely high energies, $E > -0.50\,E_h$, i.e., more than 102,000 cm^{-1} above the minimum, were discarded. The results of these fits for various orders of the two polynomials in the three-body term are shown in Tables 1 and 2. For the upper sheet, the 11th order fit is nearly as good as the 12th order fit, but for the lower sheet the 12th order fit gives quite an improvement. Therefore, we have finally chosen the 12th order expansion, with 185 linear coefficients for each sheet, as it yields highly accurate and still sufficiently compact representations of the two sheets. For completeness, the linear coefficients of these expansions are given in Table 3. The parameters of the three-body dynamical correlation energy term are listed in Table 4, those of the range determining factor, T_2, and of the expansion coordinates, $\tilde{R}_i$, in Table 5. The accuracy of the DMBE representations can be ascertained by comparison of the electronic energies at arbitrarily chosen nuclear configurations not included in the fit. To this end, 10 additional ab initio points were calculated for each of the energy ranges of the two sheets of the surface, covering a large range of nuclear configurations. The results, shown in Table 6, prove that our analytical expressions of the two sheets represent accurately the corresponding electronic energies.

The diatomic curves that enter into the two-body terms Eq. (2) require some attention. In Fig. 1 the two lowest potential curves of H_2^+, $X^2\Sigma_g^+$ and $A^2\Sigma_u^+$, are shown together with the lowest triplet curve of H_2, denoted as [20] $H_2(b^3\Sigma_u^+)$. The potential curve of the system $H_2(b^3\Sigma_u^+) + H^+$ is below that of $H_2^+(A^2\Sigma_u^+) + H$ almost everywhere. However there are shallow van der Waals minima in the diatomic potentials which make the two curves cross: In the case of $H_2(b^3\Sigma_u^+)$, a minimum with an energy of $E = -20.46\,\mu E_h$ appears at about $7.825a_0$ while for $H_2^+(A^2\Sigma_u^+)$ there is an energy minimum of $E = -65.31\,\mu E_h$ at $12.5a_0$. The crossing occurs at $R_c = 10.856a_0$. Using these two curves, we have constructed adiabatic curves by diagonalisation of the following diabatic matrix:

$$V^{(2)}_{\text{diab}}(R) = \begin{pmatrix} V_{H_2}(R) & V_{\text{od}}(R) \\ V_{\text{od}}(R) & V_{H_2^+}(R) \end{pmatrix}. \tag{24}$$

The off-diagonal element was chosen as a Gaussian function centered at the crossing point $R = R_c$,

$$V_{\text{od}}(R) = a\exp[-\gamma(R - R_c)^2] \tag{25}$$

with $\gamma = 0.5a_0^{-2}$ and $a = 2.0 \times 10^{-5}\,E_h$. The resulting adiabatic curves are shown in Fig. 2. In our previous work [2] we have used the diatomic potential curve of triplet H_2 throughout, which due to the shallowness of the van der Waals minima provides a very good approximation to the true adiabatic curve obtained here.

Table 1
Results of our fitting experiments for the lower sheet

Order		Number of coefficients	χ^2				
N	M		Range 1 209 (10)	Range 2 594 (5)	Range 3 882 (1)	Range 4 480 (1)	Range 5 1456 (1)
9	8	94	4.77	7.82	29.95	44.21	34.16
10	9	120	2.67	5.54	16.50	28.81	24.55
11	10	150	2.91	5.48	14.28	22.21	22.99
12	11	185	1.27	2.81	9.56	16.05	15.02

The energy ranges, displayed in the second line, are $E < -1.1026$ (range 1), $-1.1026 < E < -1.08$ (range 2), $-1.08 < E < -1.04$ (range 3), $-1.04 < E < -1.02$ (range 4), $E > -1.02$ (range 5). All energies are in Hartree units. In the third line we give the number of data points within the respective range and, in parentheses, the weights used in the fitting procedure. The main entries are the root mean square deviations in wave numbers.

Table 2
Results of our fitting experiments for the upper sheet

Order		Number of coefficients	χ^2			
N	M		Range 1 167 (10)	Range 2 942 (5)	Range 3 891 (2)	Range 4 327 (1)
9	8	94	4.73	9.95	18.13	38.59
10	9	120	3.37	7.05	13.13	24.65
11	10	150	3.25	6.40	13.03	24.24
12	11	185	3.05	6.35	11.02	24.18

The energy ranges, displayed in the second line, are $E < -1.01$ (range 1), $-1.01 < E < -1.00$ (range 2), $-1.00 < E < -0.96$ (range 3), $-0.96 < E < -0.92$ (range 4). The entries have the same meaning as in Table 1.

Table 3
Parameters of the three-body EHF term

i	j	k	$c_{ijk,l}^1$	$c_{ijk,l}^2$	$c_{ijk,u}^1$	$c_{ijk,u}^2$
0	0	0	0.30122377155372	−0.28935330507586	0.30122377155372	0.28935330507586
1	0	0	−0.54697403683478	−0.01402842950806	−0.54697403683478	−0.15650216030805
0	2	0	0.49726258196123	−0.14559383331206	0.79765873181720	−50.92088361618594
2	0	0	0.37557500549682	0.12712544486631	0.37557500549682	0.27973160911768
0	0	3	−0.79477856207215	3.85429546248143	1.96752537497913	−7.21088642012977
1	2	0	−0.37359021544219	0.10927091475355	−0.43962298606642	−0.77025402365138
3	0	0	−0.17416166512485	0.04400496464896	−0.17416166512485	−0.28305706959750
0	4	0	1.06084184395089	−2.97226052692556	28.57045339875761	−72.66315951465428
1	0	3	0.60495649757819	−1.32720052114982	−8.28788738434849	17.21664547564413
2	2	0	0.57608328563766	−0.18812531631956	0.20250966641852	12.40713896657378
4	0	0	0.09256922623000	−0.32386634153097	0.09256922623000	0.00262955885664
0	2	3	−10.68631406162829	16.39835739918686	18.10956552184589	−38.51315104681093
1	4	0	−0.31902479477791	0.04639556947097	−16.44277892082677	61.99889290554807
2	0	3	−0.16799475909735	−1.15891688647582	19.36725738258190	−29.28977507737056
3	2	0	−0.36388163888806	−0.67285957990138	−2.81663137985822	−4.99728510192083
5	0	0	−0.08201633440066	0.48435732989333	−0.08201633440066	0.20445866050487
0	0	6	−0.03703582903632	0.61164742964012	−1.13216249913182	7.77152665154303
0	6	0	3.82637836175714	−2.26462892807490	105.80799706513550	−104.85305605482190
1	2	3	3.91247358255366	−5.47861325897804	−18.63114049033072	41.46312839096161
2	4	0	0.01602405031625	1.49925299301221	−17.41635474710698	−4.64142849645549
3	0	3	0.04010672675937	0.93761056847833	−24.31155613518425	27.92760525700781
4	2	0	0.13443003022817	1.54704720589678	4.95191206718786	−6.03613120471341
6	0	0	0.07839428828599	−0.41151732745805	0.07839428828599	−0.17914149240040
0	4	3	−14.74207237541884	6.62426150813443	47.09852090375922	−14.38829093975993
1	0	6	−0.02168401991071	−0.17988377482680	−5.66144235157310	33.09501230172613
1	6	0	0.82722356380113	−2.71336967785496	−79.16846253558779	31.33464994422064
2	2	3	2.04751475717248	−0.01153917781829	1.03935995371920	5.97936834437824
3	4	0	−0.10348111071804	−0.00779237794571	2.96890208899606	2.21237583035730
4	0	3	0.00248192041166	−0.21613727258352	18.64285031614229	−14.85302883608863
5	2	0	−0.13358471475287	−1.26433454059637	−3.91222651415383	6.12663298039837
7	0	0	−0.05297227528534	0.22426964979776	−0.05297227528534	0.07299571631676
0	2	6	−2.08806092785418	3.93531464132131	−21.27150359678358	19.91884510642906
0	8	0	−0.14923460587272	2.71830552093002	102.72770375230930	−106.50803553961160
1	4	3	2.85372217441755	−1.30248025066946	−50.32725534807072	9.13516442719083
2	0	6	0.53197592474415	−0.45333741185624	0.81343691948798	−21.74992229853526
2	6	0	−1.47243229359787	0.41717894696250	27.37035209071646	3.42037733721745
3	2	3	−1.87573145741782	2.53669166339425	7.38721997243118	−28.75376771909166
4	4	0	−0.46023623338715	−0.33176437439251	18.31448333762220	−12.42307622551732
5	0	3	0.04729446090593	0.19065225402012	−9.57568912231895	4.13148923063669
6	2	0	0.16660605580187	0.55799663823829	1.70806662618586	−2.28807514803523
8	0	0	0.02295716346029	−0.07939786536599	0.02295716346029	−0.01423060930388
0	0	9	−0.26839326018369	1.00088531069846	1.98294350716391	−7.63037264696123
0	6	3	2.74366034560926	−6.00386875204518	−45.23247847704847	44.50652058200434
1	2	6	−1.29572028714564	2.71846079090026	−44.57493509033668	18.36980443153002
1	8	0	1.90520298979545	0.47053574733705	−3.35740903917815	14.72646258223705
2	4	3	−3.54838350423282	2.85709184530495	17.53743421048225	0.56672592952280
3	0	6	−0.56229917133659	0.83548001409323	4.60985075148112	−2.23065684017150
3	6	0	0.04697041727889	−0.30588408294335	−16.39433665197297	9.68753895874726
4	2	3	−0.68009359943781	0.08344770779551	−1.31706740762455	11.09409466721007
5	4	0	0.38949026680087	0.19644379792760	−14.10755578006616	8.93411334079022
6	0	3	−0.09656409387870	−0.08085795148344	3.42852602143602	−0.46399153183622
7	2	0	−0.11817304094414	−0.12862708697055	−0.41377218624633	0.43664311039881
9	0	0	−0.00618304688781	0.01753161047668	−0.00618304688781	0.00058194797687
0	4	6	−2.79153392519733	−0.63742665446431	−19.83175604355162	49.70488675730982
0	10	0	−3.59822262286544	1.66864332533686	69.22772362863194	−8.82968283067241
1	0	9	−0.04729337569377	0.27728674437879	−2.74627098845062	0.61641040665160
1	6	3	3.07818433726276	−1.22121476678211	17.18221941780739	−20.12984101536353
2	2	6	−0.13347133279065	−0.89696429618369	34.50629362255951	−8.61006019145325
2	8	0	0.71365917850603	−1.04558947977177	−21.68590023191552	−15.45211614005777
3	4	3	−0.43302126722225	0.51124984373962	1.80883236950235	22.71568568205576
4	0	6	0.20614674207349	−0.50161472054668	−2.75577479790481	2.71433607838544
4	6	0	0.52112932558831	−0.29478421105458	3.59573746257589	−12.91918496976746
5	2	3	0.47682970576669	−0.29439558048719	−0.88451201625561	1.37112598850917

Table 3 (continued)

i	j	k	$c^1_{ijk,l}$	$c^2_{ijk,l}$	$c^1_{ijk,u}$	$c^2_{ijk,u}$
6	4	0	−0.16171711297310	−0.06575548228785	4.09623543489712	−2.78728563143766
7	0	3	0.05642908371421	0.00077100733812	−0.83462701564850	0.01402833931997
8	2	0	0.04450552759270	0.01159108915409	0.04354693799288	−0.04724225675334
10	0	0	0.00097646010885	−0.00217757225735	0.00097646010885	0.00021271357897
0	2	9	−1.31720126021633	0.39507443503424	16.01371107076800	−8.18156086564133
0	8	3	2.07090249802489	−0.17875708599099	26.92979107927163	−27.12619716912096
1	4	6	−0.55906710077351	0.44232474328358	−15.84461983429172	4.78180216290855
1	10	0	−0.52018934182193	0.48113668527530	−7.26636379667826	3.87350205935145
2	0	9	−0.03862426072784	−0.11854851358148	2.04428879106737	−0.45150827262909
2	6	3	−2.25080433731133	−0.56397522383890	−23.87056456374641	0.35423808589387
3	2	6	0.38270974149672	0.25817704388530	−3.46950055924187	1.91362295097512
3	8	0	0.43119491459406	0.52514823479094	24.43838220956226	−0.79427866364019
4	4	3	−0.24435175102465	−0.49182070128309	−10.36814716688833	−3.83148596786202
5	0	6	−0.00504719778928	0.10416396415916	0.61780928205528	−0.29262711162053
5	6	0	−0.14420609804765	0.20028627117335	2.55402964044499	1.99602363657234
6	2	3	−0.05071755422429	−0.00216764805082	−0.08457105368633	−0.59610393632367
7	4	0	0.03839601233588	0.01312712498385	−0.44490892974665	0.31940000087168
8	0	3	−0.01263079949857	0.00172390965429	0.12252604998995	−0.00294274623376
9	2	0	−0.00828384502594	0.00005205893206	0.00149302640352	0.00278093334272
11	0	0	−0.00007885509740	0.00011551742028	−0.00007885509740	−0.00002405473809
0	0	12	−0.01692136598915		−0.09194951351961	
0	6	6	0.52745853892510		−27.75030747127519	
0	12	0	−0.31854842510948		−7.32736107968445	
1	2	9	0.02733646565819		−1.25123085470824	
1	8	3	0.88187837087510		9.56392937661069	
2	4	6	−0.33716283042862		−1.96233518568797	
2	10	0	−0.35635095447989		1.99622798418846	
3	0	9	0.03072688354360		−0.35551555817340	
3	6	3	0.79983785944692		1.29201403979359	
4	2	6	−0.11450971171883		−0.93025420297001	
4	8	0	−0.36063930912740		−2.81165062349283	
5	4	3	0.25817045445335		1.81071069832759	
6	0	6	−0.00938014758819		−0.05457654777189	
6	6	0	−0.02247159757695		−0.61063460824417	
7	2	3	0.00373950272593		0.07376030495793	
8	4	0	−0.00410975003390		0.00505774693384	
9	0	3	0.00092967703581		−0.00796615322508	
10	2	0	0.00059400934334		−0.00052712701299	
12	0	0	0.00000222005552		0.00000222005552	

Table 4
Parameters of the three-body dynamical correlation term, Eq. (5)

$\xi = 0.5$	$\eta = 3.0$	$R_{ref} = 1.5a_0$
$\lambda = 6.2$	$C_4 = -\frac{9}{2}\,E_h a_0^4$	$C_6 = -15\,E_h a_0^6$

Table 5
Parameters of the range determining factor $T_2(x)$ and of the expansion coordinates $\tilde{R}_i$, see Eqs. (12) and (14)

$\gamma = 0.5a_0^{-1}$	$x_0 = 21.0a_0$
$R_0 = 1.0a_0$	$\beta = 0.5$

Table 6
Average of deviations, given in units of cm^{-1}, between the energy values of ab initio data points not included in the fit and those obtained from our analytical representations of the two sheets

Range 1	Range 2	Range 3	Range 4	Range 5
2.13	3.06	5.64	41.58	–
1.12	3.29	6.78	6.33	6.60

Within each energy range, as defined in Tables 1 and 2, 10 data points were calculated. The first line refers to the upper sheet, while the second refers to the lower sheet.

The parameters of the diatomic potential curves for $H_2^+(X^2\Sigma_g^+)$ and $H_2(b^3\Sigma_u^+)$ were reported in [1,21], respectively. For the construction of the potential curve of the $A^2\Sigma_u^+$ state of H_2^+ we have, adopting a method proposed in [21], obtained first an analytical representation of the energy difference between the A and the X states. The potential curve for the A state is then expressed as

$$V_A^{(2)}(R) = V_X^{(2)}(R) + \exp\left(\sum_i c_i R^i\right). \quad (26)$$

Such a difference fit is preferred to the direct fit since, by ensuring that the difference term is always positive, ar-
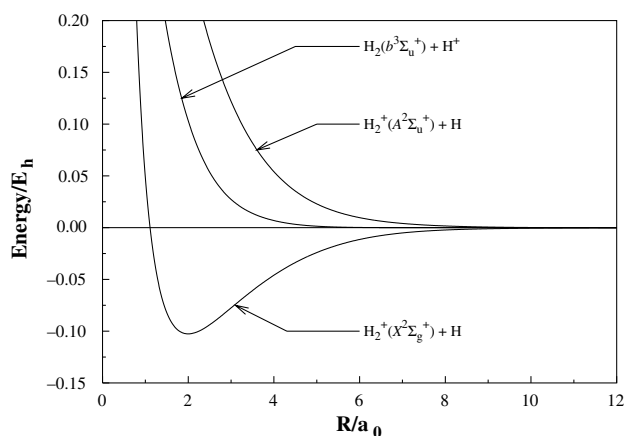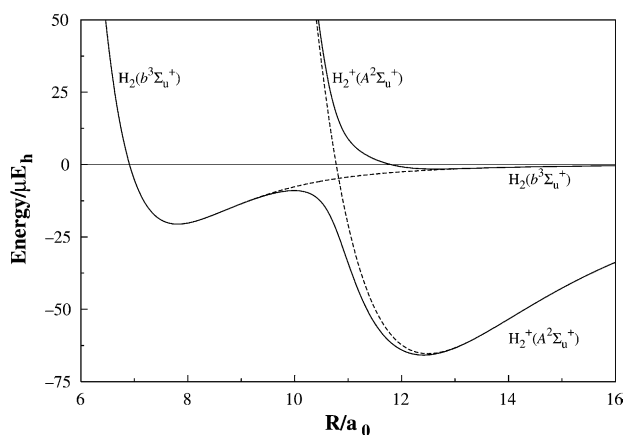
Fig. 1. Diatomic potential curves.

Fig. 2. Adiabatic and diabatic diatomic potential curves.

Table 7
Parameters of the two-body term, Eq. (27)

$c_0 = -1.061269$	$c_1 = 2.971129(-1)$	$c_2 = -4.014008(-1)$
$c_3 = 7.074256(-2)$	$c_4 = -4.632783(-3)$	

Numbers in parentheses denote powers of 10.

tificial crossing of the two potential curves can be avoided. Note that the dynamical correlation contribution is included correctly, as these contributions are identical for the two curves. The coefficients in Eq. (27) are presented in Table 7.

4. The potential energy surfaces

The two sheets of the double-valued $^3E'$ potential energy surface of H_3^+ have very different topologies. The lower sheet shows three minima at symmetric linear arrangements of the three nuclei. The three minima are equivalent, as they reflect the three possible permutations of the nuclei. The bond lengths at the minima are

$R_i = R_j = 2.4537a_0$ and $R_k = 2R_i$. These minima are separated by saddle points corresponding to C_{2v} arrangements with $R_i = R_j = 5.336a_0$ and $R_k = 1.990a_0$. The minima are stabilized by 2954.8 cm^{-1} with respect to the dissociation to $H_2^+(X^2\Sigma_g^+) + H(^2S)$. The saddle points are 359.1 cm^{-1} below this dissociation energy. The height of the saddle points with respect to the minima of the potential energy surface is thus 2595.7 cm^{-1}. The upper sheet has the form of a cone with minimum at 17876.6 cm^{-1} above the minimum of the lower sheet. The depth of the upper conical potential with respect to full dissociation to $H^+ + 2H(^2S)$ is 7596.3 cm^{-1}.

All features of the potential surfaces can be seen in the relaxed plots [22], Figs. 3 and 4. In these relaxed plots the minimum energies for fixed values of the
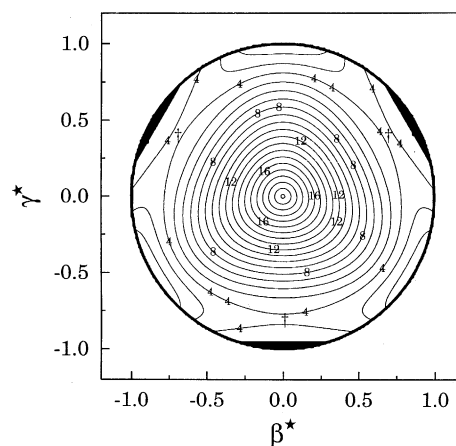

Fig. 3. Relaxed plot of the lower sheet. The first minimum can be found at $\beta^\star = 0$ and $\gamma^\star = 1$, and the other two at symmetry-related positions. The saddle points for pseudo-rotation are indicated by a dagger. Contours start at $-1.116\ E_h$, with an equal spacing of 4 mE_h.
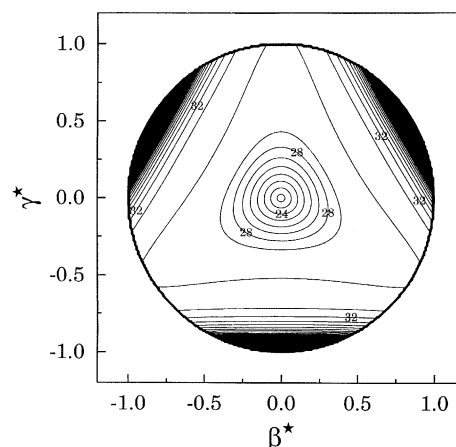

Fig. 4. Relaxed plot of the upper sheet. Contours as in Fig. 3.

hyperangles are visualized. Those angles are defined as $\beta^\star = \frac{\beta}{Q}$ and $\gamma^\star = \frac{\gamma}{Q}$, with

$$
\begin{pmatrix} Q \\ \beta \\ \gamma \end{pmatrix} = \begin{pmatrix} 1 & 1 & 1 \\ 0 & \sqrt{3} & -\sqrt{3} \\ 2 & -1 & -1 \end{pmatrix} \begin{pmatrix} R_1^2 \\ R_2^2 \\ R_3^2 \end{pmatrix}. \tag{27}
$$

Fig. 3 shows the three absolute minima at $(\beta^\star = 0, \gamma^\star = 1)$ and symmetry-related positions. The saddlepoints can be located by connecting two minima through the minimum-energy path. The corresponding figure for the upper sheet, Fig. 4, shows a regular structure. The relaxed plots also demonstrate that the surfaces are free from unphysical features. For symmetrical arrangements, this can also be seen from Fig. 5, which shows various symmetrical cuts through the two sheets together with the calculated ab initio points. Note that some of these points (the ones shown by the open circles) have not been included in the fitting procedure, although their root mean square deviations fall within the values reported for the current fit.

Figs. 6 and 7 show two different symmetric (C_{2v}) cuts through the surfaces and prove the accurate representation of the conical intersection and of the splitting between the two sheets in the vicinity of the intersection. The first of those figures, Fig. 6, represents a cut for a fixed value of the hyperradius ρ, $\rho = 4.567a_0$ and $\beta^\star = 0$. On this figure, one of the three equivalent absolute minima of the lower surface can be seen at $\gamma^\star = 1$. Here, the energy gap between the two surfaces is $\Delta E = 57567.6$ cm^{-1}. The conical intersection is located at $\gamma^\star = 0$, with energy $E_{JT} = 17995.6$ cm^{-1} with respect to the minimum. E_{JT} is referred to as the Jahn–Teller stabilization energy. The second of the two figures, Fig. 7, contains the energy values of the two sheets as a function of the bending angle ϕ, with the two equivalent bonds relaxed. The minimum of the lowest sheet is found at $\phi = 180°$, and the minimum of the conical

Fig. 6. Cut along C_{2v} arrangements for a fixed value of the hyperradius $\rho = 4.6a_0$.
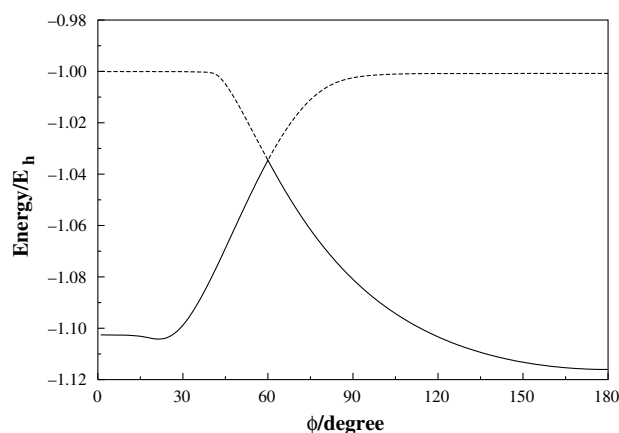
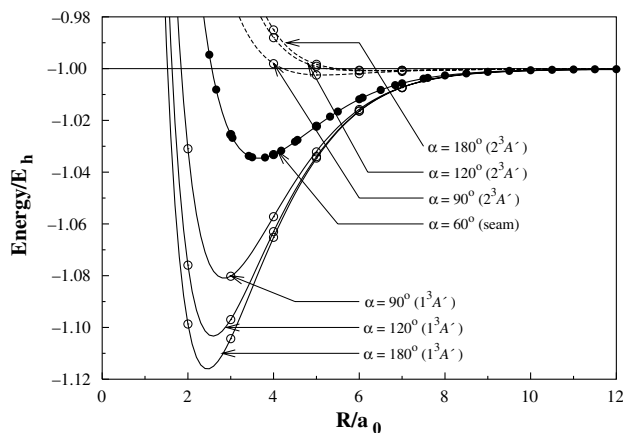Fig. 7. Minimum energy path, with bond lengths relaxed, along the bending angle.

Fig. 5. Cut along the two sheets for symmetrical arrangements as a function of the characteristic bond length. The dots indicate the calculated ab initio points: •, fitted; ○, not fitted. See also the text.
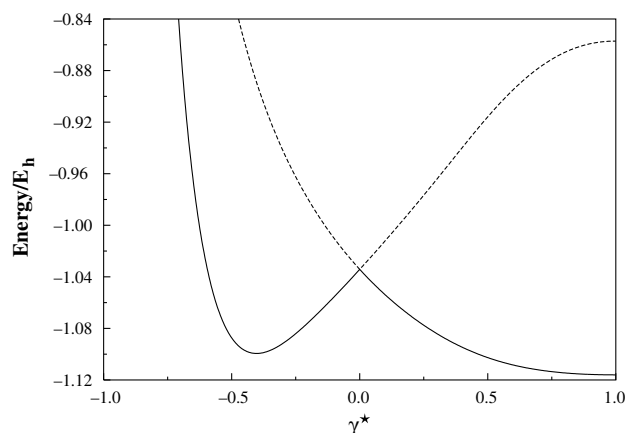
intersection at $\phi = 60°$. As we proceed towards $\phi = 0°$, we pass the saddlepoint at $\phi = 21.5°$. For smaller values of the bending angle, one bond length keeps the equilibrium distance of the H_2^+ molecule, while the other two bondlengths tend to infinity. Thus, we approach the $H_2^+(X^2\Sigma_g^+) + H(^2S)$ dissociation channel. The curve of the upper sheet attains the energy values close to $E = -1.0\ E_h$ for $\phi = 180°$ and $\phi \to 0°$. In the latter case the energy value is that of the van der Waals minimum of $H_2^+(A^2\Sigma_u^+) + H$.

Figs. 8–11 show two-dimensional plots of the two sheets as functions of two interparticle distances for fixed values of the bending angle of $\phi = 60°$, $90°$, $120°$ and $180°$. These plots show that the symmetry of the surfaces is well preserved in our analytical representations, as are their characteristic features: For example, the absolute minimum of the lower surface can be seen on the diagonal $R_1 = R_2$ of the $180°$ plot. In the $60°$ plot of the upper or lower surfaces the minimum of the conical intersection can be found on the diagonal. The
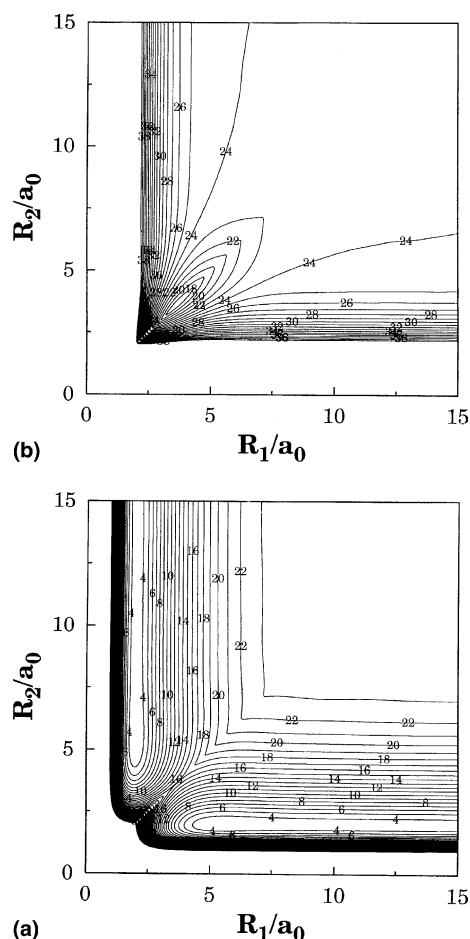
Fig. 8. Two-dimensional plots of the lower (a) and upper (b) sheets for $\phi = 60°$. Contours start at $-1.115\, E_h$, with an equal spacing of 5 mE_h.

Fig. 9. Two-dimensional plots of the lower (a) and upper (b) sheets for $\phi = 90°$. Contours as in Fig. 8.

very small kinks that show up in the upper surface plots if one of the distances is about $R \approx 10.7 a_0$ are no artefacts. They are caused by the avoided crossing in the adiabatic diatomic curves, see Fig. 2. Apart from this the contour lines are smooth, which demonstrates the quality of the analytical representations obtained here.

5. Comparison of vibronic states on the lower sheet

The lower adiabatic sheet of this surface, of $^3\Sigma_u^+$ symmetry, has received considerable attention recently. Full potential surfaces have been reported as well as studies of their vibronic [1,23,24] and ro-vibronic [25,26] states. It has been known for quite some time, through the studies by Schaad and Hicks [27], Ahlrichs et al. [28], Wormer and de Groot [29] and Preiskorn et al. [30], that this lowest triplet state is bound and should support vibrational states. In their review articles on H_3^+, both Tennyson [31] and McNab [32] emphasized the importance of the triplet state, as some of the yet unassigned lines in the hydrogen plasmas might belong to this state, and called for more detailed investigations. This call has
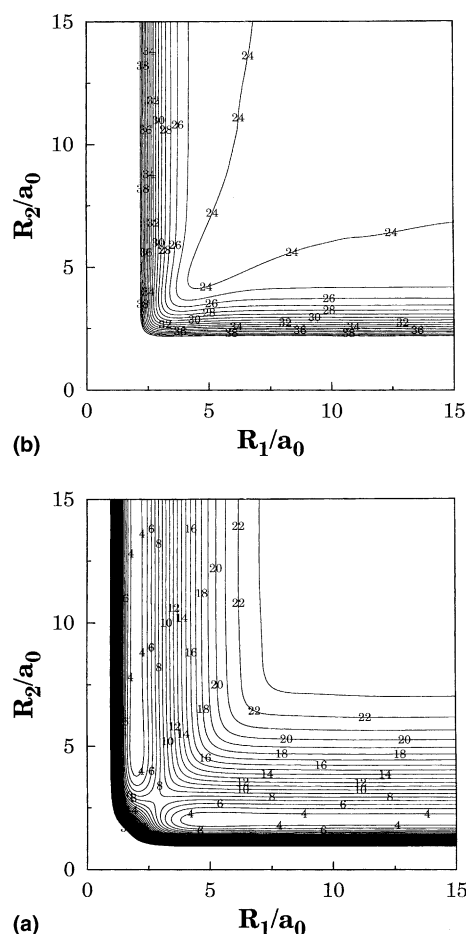
been answered only recently and led to the publication of the above-mentioned articles.

The three equivalent minima of the lower sheet, related by permutational symmetry, lead to an interesting pattern of the ro-vibronic states. Each such state has two components, one of A_1' or A_2' symmetry, the other of E' symmetry. The symmetry labels used here refer to the three-particle permutation inversion group $S_3 \times I$. This group is isomorphic to the molecular symmetry group D_{3h} (M) [33]. The two components of each ro-vibronic state do not only have different symmetry, but also different energies. The energy splitting is due to the potential barriers that separate the three minima and is negligibly small for the lowest states. For a detailed discussion of the ro-vibronic states and their symmetry properties the reader is referred to [26].

We have recalculated the vibronic states using the new analytical representation of the potential energy surface obtained here and a method based on hyperspherical harmonics [34,35] In this method, the ro-vibrational wavefunction is expanded in terms of hyperspherical harmonics, yielding a set of coupled equations in the remaining coordinate, the hyperradius.
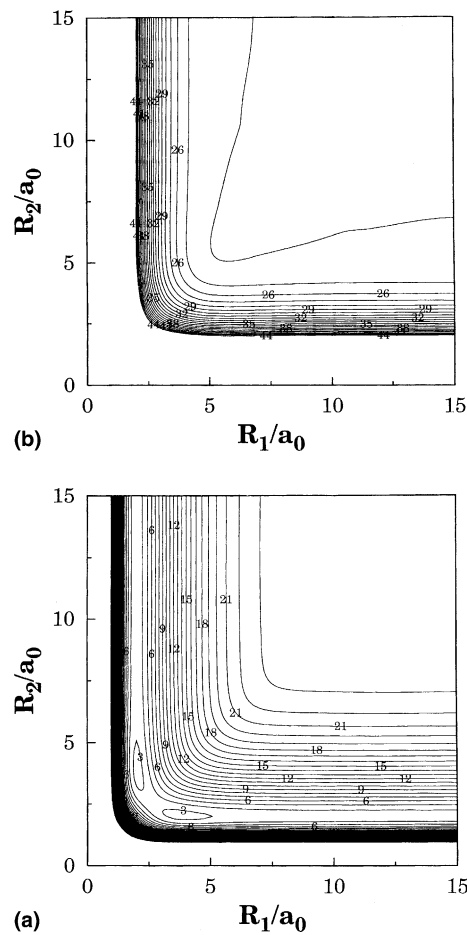
Fig. 10. Two-dimensional plots of the lower (a) and upper (b) sheets for $\phi = 120°$. Contours as in Fig. 8.
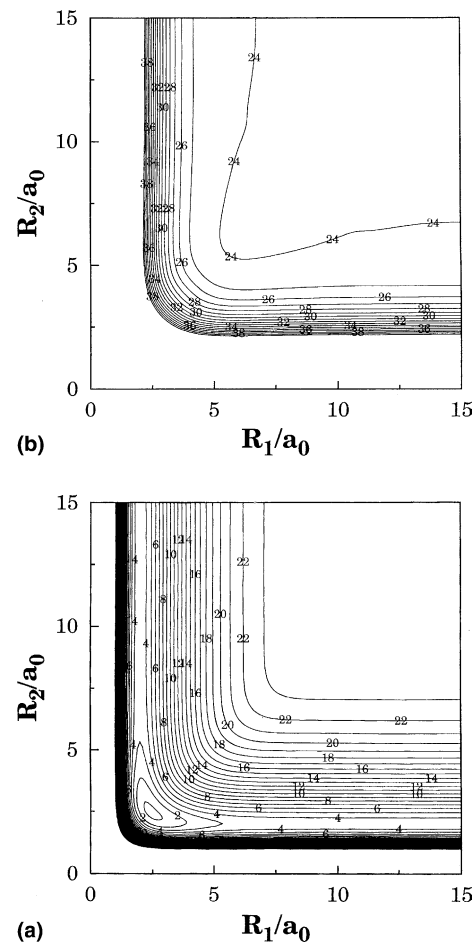
Fig. 11. Two-dimensional plots of the lower (a) and upper (b) sheets for $\phi = 180°$. Contours as in Fig. 8.

Table 8
Comparison of the vibronic energies of $^1H_3^+$ on the lower sheet of the potential energy surface

i	This work		Ref. [1]		Ref. [23]		Ref. [25]	
	A_1'/A_2'	E'	A_1'/A_2'	E'	A_1'/A_2'	E'	A_1'/A_2'	E'
0	0.00	0.00	0.00	0.00	0.00	0.00	0.00	0.00
1	738.49	738.48	739.47	739.47	736.35	736.35	738.70	738.80
2	975.05	975.05	975.50	975.50	973.83	973.83	973.00	973.10
3	1273.73	1273.79	1274.43	1274.49	1272.43	1272.49		
4	1474.50	1474.43	1475.37	1475.29	1469.08	1468.99		
5	1573.69	1573.80	1574.43	1574.54	1568.58	1568.72		
6	1730.35	1728.40	1731.74	1729.80	1726.70	1724.62		
7	1922.54	1923.04	1923.94	1924.50	1913.74	1914.43		
8	1940.32	1950.95	1942.17	1952.62	1929.08	1940.38		
9	1972.74	1970.73	1974.79	1972.83	1956.72	1954.40		
10	2158.72	2136.98	2161.05	2139.74	2143.10	2116.36		
11	2188.49	2166.97	2191.92	2169.41	2163.55	2150.23		
12	2204.85	2256.70	2207.22	2260.02	2188.39	2224.73		
13	2271.16	2262.03	2276.39	2266.01	2245.95	2241.93		
14	2312.14	2350.15	2318.71	2353.14	2286.15	2322.73		
15	2340.90	2360.19	2344.37	2363.83	2323.79	2334.73		
16	2405.21	2414.01	2418.47	2417.52	2364.73	2374.73		

Energies are in wave numbers.

This set of equations is then solved numerically with the Numerov method. Further details can be found in [1]. In these calculations, like in those mentioned above, the effect of the geometrical phase has been neglected, as it has been shown [25] for the lowest states that it is negligible.

Finally, we compare our calculated energy values of the vibrational states supported by the lower sheet of the potential energy surface with those obtained previously [1,23,25]. Such a comparison is presented in Table 8. The increased accuracy of the present fit as compared to our previous one [1] and the increased number of ab initio data points in particular in the energy region near dissociation to $H_2^+(X^2\Sigma_g^+) + H(^2S)$ manifests itself in slightly different eigenvalues. The splitting of the two components of A_1'/A_2' and E', which might become important for a future experimental study of this system, remains nearly unchanged.

6. Conclusions

In the present work, we have elaborated necessary adaptations of standard DMBE theory to describe a double-valued Jahn–Teller type potential energy surface. This theory has then been applied to the electronic a^3E' state of H_3^+. While the two sheets of this system have been investigated before in separate studies, we have now obtained an accurate description that takes into account their degeneracy at the intersection line.

Acknowledgements

References

[1] M. Cernei, A. Alijah, A. Varandas, J. Chem. Phys. 118 (2003) 2637.
[2] L.P. Viegas, M. Cernei, A. Alijah, A.J.C. Varandas, J. Chem. Phys. 120 (2004) 253.
[3] A.J.C. Varandas, Adv. Chem. Phys. 74 (1988) 255.
[4] A.J.C. Varandas, in: A. Laganá, A. Riganelli (Eds.), Lecture Notes in Chemistry, vol. 75, Springer, Berlin, 2000, p. 33.
[5] A.J.C. Varandas, in: D. Yarkony, H. Köppel, W. Domcke (Eds.), Conical Intersections: Electronic Structure, Dynamics and Spectroscopy, World Scientific, Singapore, 2003.
[6] A.J.C. Varandas, J. Chem. Phys. 105 (1996) 3524.
[7] A.J.C. Varandas, Mol. Phys. 60 (1987) 527.
[8] R.J. Le Roy, Spec. Period. Rep. Chem. Soc. Mol. Spectrosc. 1 (1973) 113.
[9] A.J.C. Varandas, J.N. Murrell, Faraday Discuss. Chem. Soc. 62 (1977) 92.
[10] H.A. Jahn, E. Teller, Proc. R. Soc. 161A (1937) 220.
[11] H. Weyl, The Classical Theory of Groups, Princeton University Press, 1946.
[12] A.J.C. Varandas, J.N. Murrell, Chem. Phys. Lett. 84 (1982) 440.
[13] J.N. Murrell, S. Carter, S.C. Farantos, P. Huxley, A.J.C. Varandas, Molecular Potential Energy Functions, Wiley, Chichester, 1984.
[14] W. Meyer, P. Botschwina, P.R. Burton, J. Chem. Phys. 84 (1986) 891.
[15] H.-J. Werner, P.J. Knowles, MOLPRO is a package of ab initio programs written by H.-J. Werner, P.J. Knowles, with contributions from R.D. Amos, A. Bernhardsson, A. Berning, P. Celani, D.L. Cooper, M.J.O. Deegan, A.J. Dobbyn, F. Eckert, C. Hampel, G. Hetzer, T. Korona, R. Lindh, W. Lloyd, S.J. McNicholas, F.R. Manby, W. Meyer, M.E. Mura, A. Nicklass, P. Palmieri, R. Pitzer, G. Rauhut, M. Schütz, H. Stoll, A.J. Stone, R. Tarroni, T. Thorsteinsson (2000).
[16] T.H. Dunning Jr., J. Chem. Phys. 90 (1989) 1007.
[17] R.C. Whitten, F.T. Smith, J. Math. Phys. 9 (1968) 1103.
[18] B.R. Johnson, J. Chem. Phys. 73 (1980) 5051.
[19] O. Friedrich, Ph.D. thesis, University of Bielefeld, Bielefeld, Germany, 2000.
[20] K.P. Huber, G. Herzberg, Molecular Spectra and Molecular Structure. IV Constants of Diatomic Molecules, Van Nostrand, New York, 1979.
[21] A.J.C. Varandas, J. Chem. Phys. 107 (1997) 867.
[22] A.J.C. Varandas, Chem. Phys. Lett. 138 (1987) 455.
[23] C. Sanz, O. Roncero, C. Tablero, A. Aguado, M. Paniagua, J. Chem. Phys. 114 (2001) 2182.
[24] E. Cuervo-Reyes, J. Rubayo-Soneira, A. Aguado, M. Paniagua, C. Tablero, C. Sanz, O. Roncero, Phys. Chem. Chem. Phys. 4 (2002) 6012.
[25] O. Friedrich, A. Alijah, Z.R. Xu, A.J.C. Varandas, Phys. Rev. Lett. 86 (2001) 1183.
[26] A. Alijah, L.P. Viegas, M. Cernei, A.J.C. Varandas, J. Mol. Spectrosc. 221 (2003) 163.
[27] L.J. Schaad, W.V. Hicks, J. Chem. Phys. 61 (1974).
[28] R. Ahlrichs, C. Votava, C. Zirc, J. Chem. Phys. 66 (1977) 2771.
[29] P.E.S. Wormer, F. de Groot, J. Chem. Phys. 90 (1989) 2344.
[30] A. Preiskorn, D. Frye, E. Clementi, J. Chem. Phys. 94 (1991) 7204.
[31] J. Tennyson, Rep. Prog. Phys. 57 (1995) 421.
[32] I. McNab, Adv. Chem. Phys. 89 (1995) 1.
[33] P.R. Bunker, P. Jensen, Molecular Symmetry and Spectroscopy, second ed., NRC Press, Ottawa, Ontario, 1998.
[34] M.I. Mukhtarova, V.D. Efros, J. Phys. A 19 (1986) 1589.
[35] L. Wolniewicz, J. Chem. Phys. 90 (1988) 371.